© 2024

QUANTUM TRANSPORT THROUGH THE GRAPHENE-SILICENE NANORIBBONS JUNCTION

M. Najarsadeghi , A. A. Fouladi [*] *, A. Z. Rostami , A. Pahlavan*

Department of Physics, Sari Branch, Islamic Azad University
4818168984 Sari, Iran

In this paper, the quantum transport through armchair graphene-silicene nanoribbons junction has been investigated by using non-equilibrium Green's function method and tight binding approximation in Landauer-Büttiker formalism. The results demonstrate that this junction exhibits metallic behavior in the absence of intrinsic spin-orbit interaction and by increasing the size of the intrinsic spin-orbit interaction, the transition from conductor to semiconductor for the system occurs. Moreover, the electron transport characteristics of the system can be controlled by changing the size of the length and width of the junction and the strength of GNR-SiNR coupling. These results can be useful for designing nanoelectronic devices.

1. INTRODUCTION

Two-dimensional hexagonal structures such as graphene and silicene have attracted a great deal of attention due to their unique electronic properties as well as their many applications in the manufacture of nanoelectronic devices [1–13]. Silicene, which is a monolayer, honeycomb structure of silicon atoms, has been successfully synthesized and many studies have been done on its electronic properties in recent years [14, 15]. Unlike graphene, silicene has no plate structure and has a buckled structure [16]. This feature of silicene is useful for adjusting the band gap, because of an external electric field effect transistors [17, 18]. Also, the spin-orbit interaction in silicene, unlike graphene, is large, which can be used to make spintronic devices [19]. Another useful feature of Silicene is its good compatibility with today's silicon-based electronics technology. Silicene nanoribbons, like graphene nanoribbons, can be divided into zigzag edges and armchair edges depending on the type of edge. The results show that the armchair silicene nanoribbons are the same as armchair graphene nanoribbons with width $N_w = 3\,m + 2$ (m is an integer) are conductive and the rest are semiconductors [20]. Recent investi-

gations have shown that hybrid nanostructures such as graphene-silicene heterostructures reveal greater physical properties than similar single graphene or silicene nanoribbons [21–26].

In this paper, electron transport through the armchair graphene-silicene nanoribbons junction (GNR-SiNR junction) has been studied numerically by using non-equilibrium Green's function and tight-binding approximation in Landauer-Büttiker formalism. The design model of this junction is shown in Fig. 1. In particular, the effect of the power of the intrinsic spin-orbit interaction, the strength of GNR-SiNR coupling, the length and width of the junction on the transmission probability function, and the electric current have been investigated.

2. METHODOLOGY

In this article, we characterize our method based on the GNR-SiNR junction consisting of armchair graphene/silicene nanoribbon as a central region (CR) contacted to two semi-infinite armchair GNR and SiNR electrodes, as shown in Fig. 1. To study the quantum transport properties of the GNR-SiNR junction, we decompose the total Hamiltonian of the system as

$$H = H_{CR} + H_R + H_L + H_C, \qquad (1)$$

where $H_{CR} = H_{GNR} + H_{SiNR} + H_{GS}$ describes the Hamiltonian of the central region, $H_R(H_L)$ is the

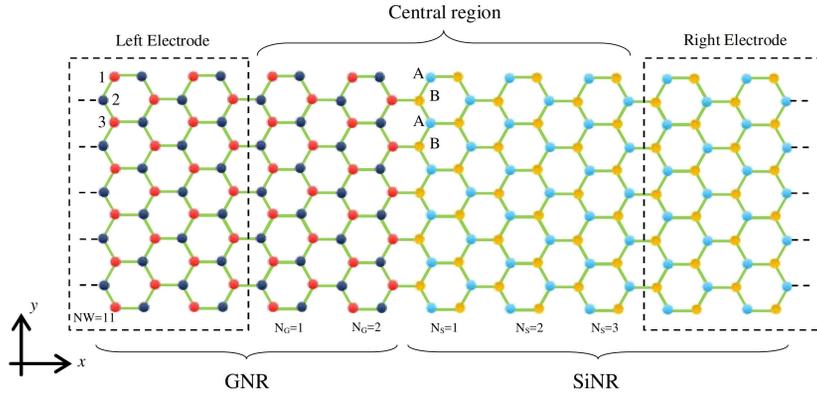[*] E-mail: a.ahmadifouladi@iausari.ac.ir

Fig. 1. Graphene nanoribbons (GNR), silicene- nanoribbons junction design. The left semi-infinite electrode is a graphene nanoribbons and the right semi-infinite electrode is a silicene nanoribbons that are connected to the central region

Hamiltonian of the right SiNR (left GNR) electrode, and H_C is the Hamiltonian for the coupling between CR and electrodes. Using the tight-binding model with nearest-neighbor hopping approximation, the Hamiltonians H_{GNR}, H_{SiNR}, and H_C can be expressed as follows:

$$H_{GNR} = \varepsilon \sum_{i,\sigma} c_{i,\sigma}^\dagger c_{i,\sigma} - t_G \sum_{i,j,\sigma} \left(c_{i,\sigma}^\dagger c_{j,\sigma} + H.c \right), \quad (2)$$

$$H_{SiNR} = -t_S \sum_{\langle ij \rangle\, \alpha} c_{i\alpha}^\dagger c_{j\alpha} +$$
$$+ i\frac{\lambda_{SO}}{3\sqrt{3}} \sum_{\langle\langle ij \rangle\rangle\, \alpha\beta} \eta_{ij}\, c_{i\alpha}^\dagger\, \sigma_{\alpha\beta}^z\, c_{j\beta} -$$
$$- i\frac{2}{3}\lambda_R \sum_{\langle\langle ij \rangle\rangle\, \alpha\beta} \xi_{ij}\, c_{i\alpha}^\dagger\, (\vec{\sigma} \times \vec{d}_{ij}^{\,0})_{\alpha\beta}^z\, c_{j\beta}, \quad (3)$$

$$H_{GS} = - \sum_{i,j,\sigma} t_{GS(i,j,\sigma)} (c_{i,\sigma}^\dagger c_{j,\sigma} + H.c), \quad (4)$$

$$H_C = \sum_{i,j,\sigma} t_{c(i,j,\sigma)} (c_{i,\sigma}^\dagger d_{j,\sigma} + H.c), \quad (5)$$

$c_{i,\sigma}^\dagger$, and $c_{i,\sigma}$ ($d_{i,\sigma}^\dagger$, and $d_{i,\sigma}$) are the creation and annihilation operators of a π-electron at the ith site of the GNR-SiNR (electrodes), respectively. i and j stand for the nearest-neighbor pairs in the GNR and SiNR lattices. ε is the on-site energy. The hopping integral between the nearest-neighbor GNR(SiNR) lattice is $t_G = 2.7\,\text{eV}$ ($t_S = 1.6\,\text{eV}$ [27]). $\langle ij \rangle$ and $\langle\langle ij \rangle\rangle$ stand for the nearest-neighbor and next nearest-neighbor pairs in the SiNR lattice, respectively. The effective intrinsic spin-orbit interaction (SOI) parameter and the intrinsic

Rashba SOI parameter are λ_{SO} and λ_R, respectively. $\vec{\sigma} = (\sigma_x, \sigma_y, \sigma_x)$ is the Pauli matrix with $\eta_{ij} = -1$ ($\eta_{ij} = +1$) if the next-nearest neighbor hopping is clockwise (anticlockwise) with respect to the positive z-axis, and $\xi_{ij} = +1$ ($\xi_{ij} = -1$) for A(B) site. $\vec{d}_{ij}^{\,0} = \frac{\vec{d}_{ij}}{|\vec{d}_{ij}|}$ is the unit vector parallel to the vector $\vec{d}_{ij}$ connecting the two sites i and j in the same sublattice. H_{GR} is the Hamiltonian for the coupling between GNR-SiNR in the central region and t_{GS} is the coupling strength between the GNR and SiNR. Also, $t_c = t_G$ ($t_c = t_S$) is the coupling strength between left GNR (right SiNR) electrode and GNR (SiNR) in the central region. The Green's function of the system is expressed as

$$G(E) = \left[(E + i\eta)I - H_{GS} - \Sigma_{L,\sigma} - \Sigma_{R,\sigma} \right]^{-1}, \quad (6)$$

where I represents the identity matrix and $\eta \to 0^+$, E is the energy of the injecting electron. Σ_L and Σ_R are the self-energy matrices due to the connection of right and left electrodes to the central region, respectively, that can be calculated numerically by the recursive method described by Sancho and co-workers [28]. The surface Green's function of the right and left electrodes are calculated as

$$g_{0,0}^L = \left[(E + i0^+)I - H_{0,0} - H_{-1,0}^\dagger \tilde{T} \right]^{-1}, \quad (7)$$

$$g_{N+1,N+1}^R = \left[(E + i0^+)I - H_{N+1,N+1} - H_{N+1,N+2}^\dagger T \right]^{-1}, \quad (8)$$

where $H_{0,0}(H_{N+1,N+1})$ and $H_{-1,0}(H_{N+1,N+2})$ are the Hamiltonian of a unit-cell and the coupling matrix between two unit cells in the left (right) electrode, respectively. Here T and $\tilde{T}$ are the transfer matrices,

which can be computed from the Hamiltonian matrix elements via an iterative procedure as [28]

$$T = t_0 + \tilde{t}_0 t_1 + \tilde{t}_0 \tilde{t}_1 t_2 + ... + \tilde{t}_0 \tilde{t}_1 \tilde{t}_2 ... t_m, \quad (9)$$

$$\tilde{T} = \tilde{t}_0 + t_0 \tilde{t}_1 + t_0 t_1 \tilde{t}_2 + ... + t_0 t_1 t_2 ... \tilde{t}_m, \quad (10)$$

where t_i and $\tilde{t}_i$ with $1 \leq i \leq m$ are defined by recursion formulas

$$t_i = (I - t_{i-1}\tilde{t}_{i-1} - \tilde{t}_{i-1}t_{i-1})^{-1} t_{i-1}^2, \quad (11)$$

$$\tilde{t}_i = (I - t_{i-1}\tilde{t}_{i-1} - \tilde{t}_{i-1}t_{i-1})^{-1} \tilde{t}_{i-1}^2. \quad (12)$$

The following conditions are applied to calculate $\tilde{t}_i$ and t_i in Eq. (8) for the left electrode

$$\tilde{t}_0 = \left[(E + i0^+)I - H_{0,0} \right]^{-1} H_{-1,0}^\dagger, \quad (13)$$

$$t_0 = \left[(E + i0^+)I - H_{0,0} \right]^{-1} H_{-1,0}, \quad (14)$$

and for the right electrode in Eq. (9)

$$\tilde{t}_0 = \left[(E + i0^+)I - H_{N+1,N+1} \right]^{-1} H_{N+1,N+2}^\dagger, \quad (15)$$

$$t_0 = \left[(E + i0^+)I - H_{N+1,N+1} \right]^{-1} H_{N+1,N+2}. \quad (16)$$

The iteration is repeated until $\tilde{t}_m, t_m \leq \delta$ with δ arbitrarily small. Finally, we can calculate the self-energies of the two left and right electrodes by

$$\Sigma_L = H_{0,1}^\dagger g_{0,0}^L H_{0,1}, \quad (17)$$

$$\Sigma_R = H_{N,N+1} g_{N+1,N+1}^R H_{N,N+1}^\dagger. \quad (18)$$

The energy-dependent transmission function in terms of the Green's function of the central region and the coupling of it with two left and right electrodes can be written as

$$T(E) = Tr(\Gamma_L(E) G^r(E) \Gamma_R(E) G^a(E)). \quad (19)$$

Where G^r (G^a) is the retarded (advanced) Green's function, and $\Gamma_{L(R)} = i(\Sigma_{L(R)} - \Sigma_{L(R)}^\dagger)$ is the coupling matrix. The electric current can be calculated by the Landauer–Büttiker formula [29]:

$$I(V) = \frac{e}{h} \int\limits_{-\infty}^{+\infty} T(E) \left[f_L - f_R \right] dE \quad (20)$$

where $f_{L(R)} = f(E - \mu_{L(R)})$ is the Fermi–Dirac distribution functions in the left (right) electrode with chemical potential $\mu_{L(R)} = E_F \pm \frac{eV}{2}$ and Fermi energy E_F.
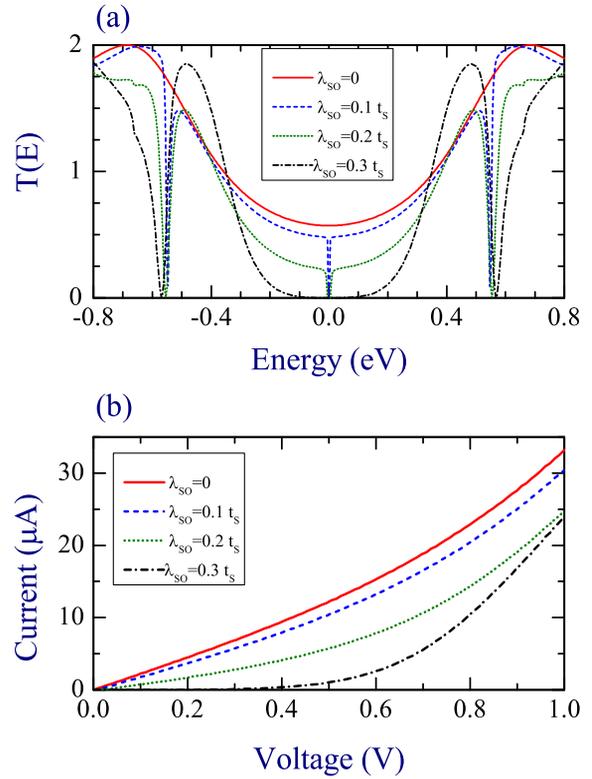

Fig. 2. a — Transmission function as a function of energy. b — The current-voltage characteristic for different values of λ_{SO} with $N_W = 11$, $N_S = 5$, $N_G = 5$

3. RESULTS AND DISCUSSION

In this section, we represent the results of the numerical calculations of the quantum transport of the GNR-SiNR system. The Fermi energy and temperature are chosen $E_F = 0$, $T = 4K$ respectively. Also, the intrinsic Rashba SOI parameter is $\lambda_R = 0.7\,\text{meV}$ [27]. The intrinsic and intrinsic Rashba spin-orbit interactions in graphene is omitted since it is negligible compared to the one in silicene [30, 31].

3.1. The effects of spin-orbit interaction

Figures 2 a, b illustrate the diagram of electron transmission probability in terms of energy and electric current in terms of bias voltage, respectively, for different values of λ_{SO} with $N_W = 11$, $N_S = 5$, $N_G = 5$. As it is shown in Fig. 2 a, the transmission probability diagram has oscillating behavior; whereas for a junction that all its parts are composed of graphene or silicene nanoribbons, the transmission function has a step form. This is due to the effect of quantum interference, which occurs due to the scattering of electron waves at the

junction of graphene and silicene nanoribbons due to the mismatch of transmission modes in these locations. In the transmission probability diagram, the resonant peaks are symmetrically located around the Dirac point ($E = 0$). In the absence of intrinsic spin-orbit interaction ($\lambda_{SO} = 0$), the probability of transmission at the Dirac point has a non-zero value, which indicates that the system is conductive. By increasing the value of λ_{SO}, it is observed that the probability of transmission at the Dirac point decreases and $\lambda_{SO} = 0.3t_s$ reaches zero and the gap in transmission function (the zero range of the transmission function around the Dirac point) appears. Thus, by increasing the λ_{SO} value, we see the transition from conductive to semiconductor for the system. Also, for $\lambda_{SO} \neq 0$ the probability of transmission in the energy range ± 0.5 eV$< E < \pm 0.5$ eV has a valley, which is called the anti-resonance state and is due to the destructive interference between the propagated states along the nanoribbons for the presence of spin-orbit interaction. As λ_{SO} increases, the amplitude of these anti-resonance modes increases. The important point is that for a system in which all parts (electrodes and central region) are composed of graphene nanoribbons, the transmission probability diagram has no gaps and the system is conductive. It also remains conductive for a system in which all parts are made of silicene nanoribbons, even in the presence of an intrinsic spin-orbit interaction. Therefore, by connecting graphene and silicene nanoribbons, a junction can be designed that has the property of switching from conductive to the semiconductor. We now interpret the current-voltage characteristic in Fig. 2 b. For λ_{SO}, there is no threshold voltage to turn on the current because of the lack of a gap in the transmission probability diagram. As λ_{SO} increases, the size of the current decreases due to a decrease in the probability of transmission near the Dirac point(-0.3 eV$< E < 0.3$ eV).As the λ_{SO} increases due to the appearance of the emission function gap, the magnitude of the threshold voltage to turn on the current also increases.

3.2. The study of geometric factors

Figure 3 investigates the effect of nanoribbon length on the electron transport properties for $N_W = 11$, $\lambda_{SO} = 0.2t_s$ values. In this case, we consider the length of the graphene nanoribbons to be constant($N_G = 5$) and the length of the silicene nanoribbons(N_S) to be variable. As it is shown in Fig. 3 a, The nearest resonance peaks to the Dirac point move towards the Dirac point with the increase of N_S and the width of these peaks also decreases. However, the magni-
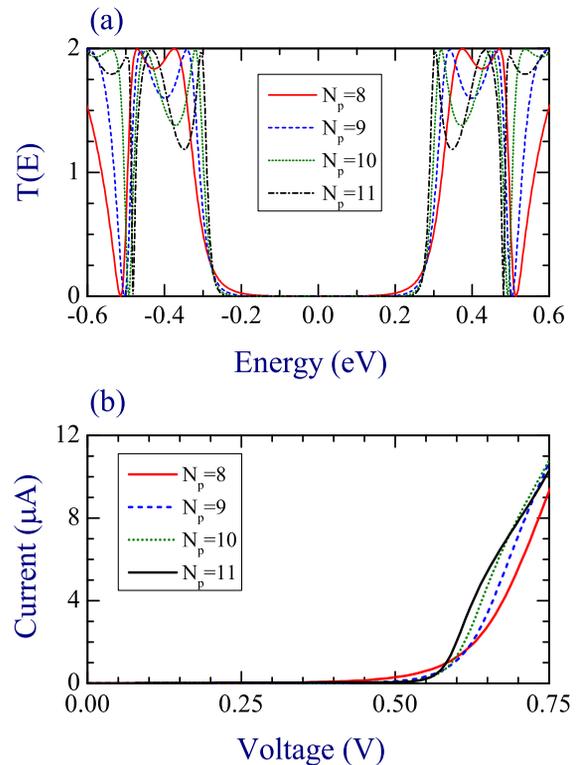

Fig. 3. a — Transmission function as a function energy. b — The current-voltage characteristic for different N_S values with $N_W = 11$, $N_G = 5$, $\lambda_{SO} = 0.2t_s$

tude of the probability of transmission near the Dirac point (-0.27 eV$< E < 0.27$ eV) decreases with increasing length. As a result of the gap, the probability of transmission increases with the increase of N_S. The effect of this gap increase is reflected in the diagram in a way that the threshold voltage increases with increasing N_S (see Fig. 3 a).

In Fig. 4, we investigated the effect of nanoribbon's width (N_W) size on the system's electronic transport for $N_W = 11$, $N_S = 5$, $\lambda_{SO} = 0.2t_s$ values. Figure 4 a represents the diagram of the energy transmission probability in terms of energy for different widths of the junction. As it is observed, as the width of the junction increases, the magnitude of the transmission probability decreases around the Dirac point (-0.35 eV$< E < 0.35$ eV), and the magnitude of the transmission probability gap increases (internal figure of Fig. 4 a). Also, the transmission function valleys approach the Dirac point by increasing the width of the nanoribbons. In Fig. 4 b, the effect of nanoribbon's width size on current-voltage characteristics is plotted. It is observed that with increasing the width of the nanoribbons, the threshold voltage increases, also
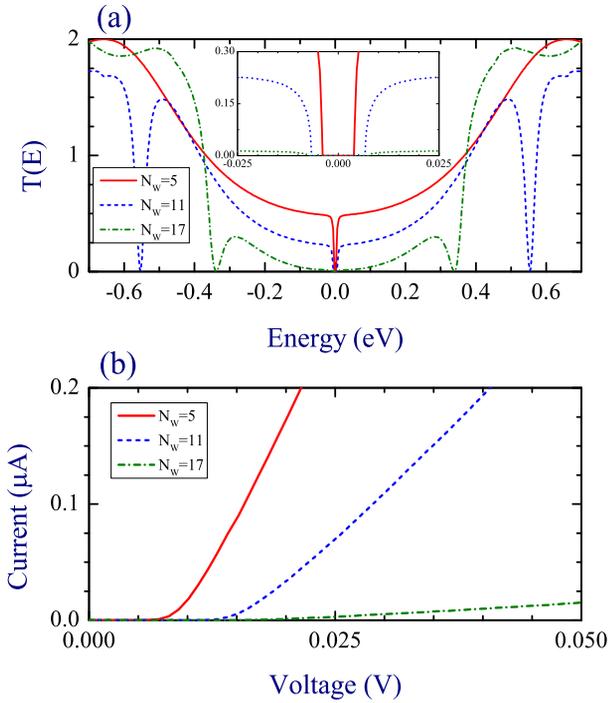
Fig. 4. a — Transmission function as a function energy. b — The current-voltage characteristic for different N_W values with $N_G = 5$, $N_S = 5$, $\lambda_{SO} = 0.2t_s$

Fig. 5. a — Transmission function as a function energy. b — The current-voltage characteristic for different t_{GS} values with $N_W = 0$, $N_G = 5$, $N_S = 5$, $\lambda_{SO} = 0.2t_s$

the current size decreases. Therefore, by changing the geometry (length and width) of the nanoribbons, the electron transport characteristics of the system can be controlled.

3.3. The effect of the strength of GNR-SiNR coupling

Figure 5 investigates the effect of the strength of GNR-SiNR coupling (t_{GS}) on the electron transport properties of the system for $N_W = 0$, $N_G = 5$, $N_S = 5$, $\lambda_{SO} = 0.2t_s$. With the increase of t_{GS}, the antiresonance dips become wider and smaller and approach zero energy (see Fig. 5 a). Also the antiresonance dip at the zero energy becomes smaller. As a result, the current decreases with the increase of t_{GS} as seen in Fig. 5 b. This result shows how we can control the quantum transport of the system by changing the strength of GNR-SiNR coupling.

4. CONCLUSION

In this paper, the electron transport through the graphene-silicene nanoribbons junction is investigated
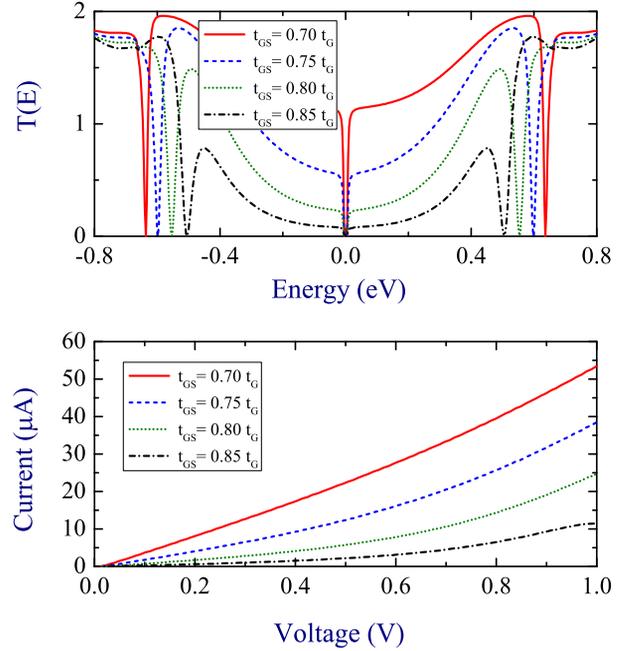
using the non-equilibrium Green's function method and tight-binding approximation in the Landauer-Büttiker formalism. The results show that the electron transport characteristics of the junction are very sensitive to the power of the intrinsic spin-orbit interaction quantity as well as the geometry (length and width) of the junction. In the presence of an intrinsic spin-orbit interaction quantity, the transmission function gap is created and the conductor to the semiconductor transition occurs. As the transmission function gap increases, the threshold voltage magnitude in the current-voltage characteristic increases. As the length of the junction increases, the width of the nearest resonant peaks to the Dirac point decreases and they move towards the Dirac point. The transmission probability gap also increases with increasing length, resulting in an increase in the threshold voltage magnitude. As the width of the nanoribbons increases, the magnitude of the transmission probability around the Dirac point decreases, the gap size of the transmission probability increases, and the valleys of the transmission function approach the Dirac point. Consequently, the magnitude of the electric current decreases, and the magnitude of the threshold voltage increases. These results can be used to control electron transport in nanoelectronic devices.

REFERENCES

1. M. Brzezinska, Y. Guan, O. V. Yazyev, S. Sachdev, and A. Kruchkov, *Engineering Syk Interactions in Disordered Graphene Flakes Under Realistic Experimental Conditions*, Phys. Rev. Lett. **131**, 036503 (2023), doi:10.1103/PhysRevLett.131.036503.

2. Y.-Z. Chou and S. Das Sarma, *Kondo Lattice Model in Magic-Angle Twisted Bilayer Graphene*, Phys. Rev. Lett. **131**, 026501 (2023), doi:10.1103/PhysRevLett.131.026501.

3. S. Jois, J. L. Lado, G. Gu, Q. Li, and J. U. Lee, *Andreev Reflection and Klein Tunneling in High-Temperature Superconductorgraphene Junctions*, Phys. Rev. Lett. **130**, 156201 (2023), doi:10.1103/PhysRevLett.130.156201.

4. C. Lu, Y. Gao, X. Cao, Y. Ren, Z. Han, Y. Cai, and Z. Wen, *Linear and Nonlinear Edge and Corner States in Graphenelike Moire Lattices*, Phys. Rev. B **108**, 014310 (2023), doi:10.1103/PhysRevB.108.014310.

5. G. Yu, Y. Wang, M. I. Katsnelson, and S. Yuan, *Origin of the Magic Angle in Twisted Bilayer Graphene From Hybridization of Valence and Conduction Bands*, Phys. Rev. B **108**, 045138 (2023), doi:10.1103/PhysRevB.108.045138.

6. M. Najarsadeghi, A. Ahmadi Fouladi, A. Z. Rostami, and A. Pahlavan, *Tunnel Magnetoresistance of Trilayer Graphene-Based Spin Valve*, Phys. E **144**, 115422 (2022), doi:10.1016/j.physe.2022.115422.

7. A. A. Fouladi, *Spin-Dependent Transport Properties of Aa-Stacked Bilayer Graphene Nanoribbon*, Phys. E **102**, 117 (2018), doi:10.1016/j.physe.2018.05.002.

8. A. A. Fouladi, *Effect of Uniaxial Strain on the Tunnel Magnetoresistance of T-Shaped Graphene Nanoribbon Based Spinvalve*, Superlattices and Microstructures **95**, 108 (2016), doi:10.1016/j.spmi.2016.04.043.

9. A. A. Fouladi and S. Ketabi, *Electronic Properties of Z-Shaped Graphene Nanoribbon Under Uniaxial Strain*, Phys. E **74**, 475 (2015), doi:10.1016/j.physe.2015.08.018.

10. G. Le Lay, *Silicene Transistors*, Nature Nanotech. **10**, 202 (2015), doi:10.1038/nnano.2015.10.

11. H. Emami-Nejad, A. mir, Z. Lorestaniweiss, A. Farmani, and R. Talebzadeh, *First Designing of a Silicene-Based Optical Mosfet With Outstanding Performance*, Sci. Rep. **13**, 6563 (2023), doi:10.1038/s41598-023-33620-2.

12. A. A. Fouladi, *Electronic Transport Properties of T-Shaped Silicene Nanoribbons*, Phys. E **91**, 101 (2017), doi:10.1016/j.physe.2016.10.040.

13. A. A. Fouladi, *Quantum Transport Through a Z-Shaped Silicene Nanoribbon*, Chinese Phys. B **26**, 047304 (2017), doi:10.1088/1674-1056/26/4/047304.

14. B. Lalmi, H. Oughaddou, H. Enriquez, A. Kara, S. Vizzini, B. Ealet, and B. Aufray, *Epitaxial Growth of a Silicene Sheet*, Appl. Phys. Lett. **97**, 223109 (2010), doi:10.1063/1.3524215.

15. C. Grazianetti, E. Cinquanta, and A. Molle, *Two-Dimensional Silicon: The Advent of Silicene*, 2D Materials **3**, 012001 (2016), doi:10.1088/2053-1583/3/1/012001.

16. P. Vogt, P. Padova, C. Quaresima, J. Avila, E. Frantzeskakis, M. Asensio, A. Resta, B. Ealet, and G. Le Lay, *Silicene: Compelling Experimental Evidence for Graphenelike Two-Dimensional Silicon*, Phys. Rev. Lett. **108**, 155501 (2012), doi:10.1103/PhysRevLett.108.155501.

17. M. Ezawa, *A Topological Insulator and Helical Zero Mode in Silicene Under an Inhomogeneous Electric Field*, New J. Phys. **14**, 033003 (2012), doi:10.1088/1367-2630/14/3/033003.

18. N. Drummond, V. Zolyomi, and V. Falko, *Electrically Tunable Band Gap in Silicene*, Phys. Rev. B **85**, doi:10.1103/PhysRevB.85.075423.

19. Z. Zhu, Y. Cheng, U. Schwingenschlogl, *Giant Spin-Orbit-Induced Spin Splitting in Two-Dimensional Transition-Metal Dichalcogenide Semiconductors*, Phys. Rev. B **84**, 153402 (2011), doi:10.1103/PhysRevB.84.153402.

20. Y. Ding and J. Ni, *Electronic Structures of Silicon Nanoribbons*, Applied Phys. Lett. **95**, 083115 (2009), doi:10.1063/1.3211968.

21. B. Kiraly, A. J. Mannix, M. C. Hersam, and N. P. Guisinger, *Graphene-silicon Heterostructures at the Two-Dimensional Limit*, Chemistry of Materials **27**, 6085 (2015), doi:10.1021/acs.chemmater.5b02602.

22. L. Meng, Y. Wang, L. Li, and H.-J. Gao, F*Abrication of Graphene-silicon Layered Heterostructures by Carbon Penetration of Silicon Film*, Nanotechnology **28**, 084003 (2017), doi:10.1088/1361-6528/aa53cf.

23. G. Li, L. Zhang, W. Xu, J. Pan, S. Song, Y. Zhang, H. Zhou, Y. Wang, L. Bao, Y.-Y. Zhang, S. Du, M. Ouyang, S. T. Pantelides, and H.-J. Gao, *Stable Silicene in Graphene/silicene Van Der Waals Heterostructures*, Advanced Materials **30**, 1804650 (2018), doi:10.1002/adma.201804650.

24. B. Liu, J. A. Baimova, C. D. Reddy, S. V. Dmitriev, W. K. Law, X. Q. Feng, and K. Zhou, *Interface Thermal Conductance and Rectification in Hybrid Graphene/silicene Monolayer*, Carbon **79**, 236 (2014), doi:10.1016/j.carbon.2014.07.064.

25. H. Pourmirzaagha and S. Rouhi, *Molecular Dynamic Simulations of the Heat Transfer in Double-Layered Graphene/Silicene Nanosheets*, Phys. B **666**, 415079 (2023), doi:10.1016/j.physb.2023.415079.

26. J. Zhou, H. Li, H.-K. Tang, L. Shao, K. Han, and X. Shen, *Phonon Thermal Transport in Silicene/graphene Heterobilayer Nanostructures: Effect of Interlayer Interactions*, ACS Omega **7**, 5844 (2022), doi:10.1021/acsomega.1c05932.

27. C.-C. Liu, H. Jiang, and Y. Yao, *Low-Energy Effective Hamiltonian Involving Spin-Orbit Coupling in Silicene and Two-Dimensional Germanium and Tin*, Phys. Rev. B **84**, 195430 (2011), doi:10.1103/PhysRevB.84.195430.

28. M. P. L. Sancho, J. M. L. Sancho, J. M. L. Sancho, and J. Rubio, *Highly Convergent Schemes for the Calculation of Bulk and Surface Green Functions*, J. Phys. F: Metal Physics **15**, 851 (1985), doi:10.1088/0305-4608/15/4/009.

29. S. Datta, *Electronic Transport in Mesoscopic Systems*, Cambridge University Press, Cambridge (1995).

30. J. C. Boettger and S. B. Trickey, *First-Principles Calculation of the Spin-Orbit Splitting in Graphene*, Phys. Rev. B **75**, 121402 (2007), doi:10.1103/PhysRevB.75.121402.

31. H. Min, J. E. Hill, N. A. Sinitsyn, B. R. Sahu, L. Kleinman, and A. H. Mac- Donald, *Intrinsic and Rashba Spin-Orbit Interactions in Graphene Sheets*, Phys. Rev. B **74**, 165310 (2006), doi:10.1103/PhysRevB.74.165310.